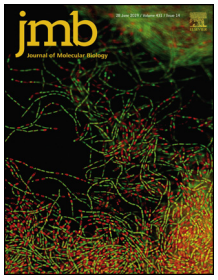

The Role of Pyrophosphorolysis in the Initiation-to-Elongation Transition by *E. coli* RNA Polymerase

Masahiko Imashimizu [1], Maria L. Kireeva [2], Lucyna Lubkowska [2], Mikhail Kashlev [2] and Nobuo Shimamoto [3,4]

1 - Molecular Profiling Research Center for Drug Discovery, *National Institute of Advanced Industrial Science and Technology, Koto-ku, Tokyo 135-0064, Japan*
2 - RNA Biology Laboratory, *Center for Cancer Research, National Cancer Institute, Frederick, MD 21702, USA*
3 - National Institute of Genetics, *Mishima, Shizuoka 411-8540, Japan*

Correspondence to Masahiko Imashimizu or Nobuo Shimamoto: *m.imashimizu@aist.go.jp, nshima@nig.ac.jp*
https://doi.org/10.1016/j.jmb.2019.04.020
Edited by M Gottesman

Abstract

RNA polymerase can cleave a phosphodiester bond at the 3′ end of a nascent RNA in the presence of pyrophosphate producing NTP. Pyrophosphorolysis has been characterized during elongation steps of transcription where its rate is significantly slower than the forward rate of NMP addition. In contrast, we report here that pyrophosphorolysis can occur in a millisecond time scale during the transition of *Escherichia coli* RNA polymerase from initiation to elongation at the *psbA2* promoter. This rapid pyrophosphorolysis occurs during productive RNA synthesis as opposed to abortive RNA synthesis. Dissociation of σ^{70} or RNA extension beyond nine nucleotides dramatically reduces the rate of pyrophosphorolysis. We argue that the rapid pyrophosphorolysis allows iterative cycles of cleavage and re-synthesis of the 3′ phosphodiester bond by the productive complexes in the early stage of transcription. This iterative process may provide an opportunity for the σ^{70} to dissociate from the RNA exit channel of the enzyme, enabling RNA to extend through the channel.

Introduction

RNA polymerases (RNAPs) can shorten the nascent RNA in a reaction of pyrophosphorolysis, which requires pyrophosphate (PPi) and leads to removal of an NMP from the 3′ RNA end. Pyrophosphorolysis has also been demonstrated for DNA polymerases and single-subunit RNAPs [1,2]. Although pyrophosphorolysis by bacterial and eukaryotic RNAPs is typically much slower than NMP addition [3–5], its rate is modulated by local DNA sequence and transcription factors [3–9]. Recent single-molecule analysis showed that PPi affects elongation by *Escherichia coli* RNAP by increasing dwell times of the elongation complex at many DNA positions [10], suggesting that pyrophosphorolysis may globally regulate transcription rate *in vivo*.

A number of regulatory mechanisms of transcription have been elucidated by assembling transcription elongation complexes *in vitro* using single-stranded DNA and RNA oligonucleotides and purified RNAP protein [11,12]. This approach is based on the ability of *E. coli* RNAP holoenzyme to bind to a single-stranded template DNA hybridized to a complementary ~9-nucleotides (nt) RNA followed by incorporation of the non-template DNA strand. The approach generates an active ternary complex (TC). The major σ subunit (σ^{70}) is released from the holoenzyme upon binding to the RNA–DNA hybrid [12]. Notably, the catalytic properties of the assembled TC are similar to those obtained from promoter, when the nascent RNA reaches the length of 20 nt [13].

On the other hand, promoter-initiated TCs carrying the 9-nt transcript (TC9; where 9 indicates the RNA length) have been shown to adopt a structurally heterogeneous state during transition from initiation to elongation [14–16]. They have been shown to adopt productive or nonproductive state called the moribund complex that can produce only short abortive RNAs without generating full-length

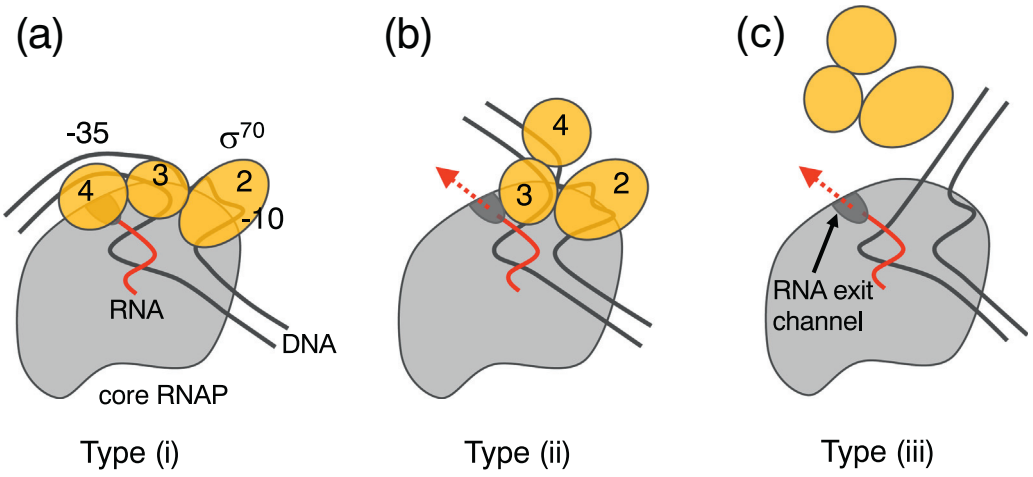

Fig.1. A structural model illustrating the transition from initiation to elongation. Panels a–c correspond to the type (i), (ii), and (iii) complex described in main text, respectively. σ^{70} 3.2 loop is not shown because its location is unidentified when the nascent RNA length is 9 nt. The entry of 5′ RNA end to the RNA exit channel (also termed single-strand RNA binding channel) begins at the RNA length of ~9–11 nt until the channel is fully filled at the RNA length of ~14–16 nt [20–22]. Since such RNA lengths should further fluctuate among TC molecules during the transition, TC9 may form all the three structural forms. Murakami and Darst's [23] crystal structures are used as a reference.

products [17–19]. Before escaping from the promoter, the productive complexes pass through multiple structural states characterized by different interactions between σ^{70} and the RNAP core complex: (i) with σ^{70} fully retained in the complex and with the 5′ RNA exit channel of RNAP occupied by the σ region 4 and 3.2 loop (Fig. 1a) [23–26]; or (ii) with σ^{70} partially retained in the TC, and σ^{70} regions 4 and 3.2 are displaced from the RNA exit channel (Fig. 1b) [20]; or (iii) without σ^{70} (Fig. 1c) [17,27]. Transition in these interactions may depend on the promoter sequence and the nascent RNA structure [15,28].

Interestingly, previous studies showed that the type (i) complex has special conformational and energetic properties: the elongation of the nascent RNA beyond ~9 nt is prevended due to blocking the RNA exit channel by σ^{70} regions 4 and 3.2 (Fig. 1a) [20]. Since σ^{70} region 4 remains bound to −35 box in the promoter DNA and to RNAP, the RNAP moving downstream during RNA synthesis causes DNA scrunching as the downstream DNA is pulled into core RNAP [29,30], and distortion energy accumulates within TC during forward translocation [14]. The more recent crystal structure of the type (i) complex of *E. coli* RNAP, which carries PPi, suggests that the DNA scrunching causes a substantial conformational change around the active site that favors PPi binding [31]. Taken together, these data raise a question of whether pyrophosphorolysis is specifically promoted in TC9 by this type (i) of conformational scrunching.

Here we demonstrate that the promoter-initiated TC9 formed by *E. coli* RNAP holoenzyme, carrying σ^{70}, contains a fraction with a strikingly fast millisecond pyrophosphorolysis rate [TC9 + PPi ➔ TC8 + ribonucleoside triphosphate (NTP)] that exceeds the elongation rate by the same complex (TC9 + NTP ➔ TC10 + PPi). We further showed that the rate of pyrophosphorolysis decreases after σ^{70} dissociates from TC9. We argue that rapid and iterative conversions between TC8 and TC9 that occur as a result of rapid pyrophosphorolysis may play a key role in displacement of σ^{70} region 4 from the RNA exit channel, preventing the arrest of initiation-to-elongation transition in the productive complex.

Results

TC with 9-nt RNA has a fraction highly susceptible to PPi

We prepared TC9 with *E. coli* RNAP by initiation on cyanobacterial *psbA2* promoter in the presence of γ-^{32}P-labeled ATP, UTP, and CTP (Fig. 2a). The *psbA2* promoter is recognized by *E. coli* RNAP *in vitro* with a similar efficiency to cyanobacterial RNAP [32]. The RNA synthesis ceased at +9C due to the lack of GTP substrate (Fig. 2a and b). In this promoter-initiated setup, σ^{70} is stochastically released from the complex [16], thereby generating a mixture of the regular TC9 and σ^{70}-associated TC9, which we call p-TC9 (Fig. 2b). In parallel, TC9 was assembled with the hybrid composed of the same 5′-labeled 9-nt RNA and a DNA without transcription. It was previously reported that σ^{70} was fully released from this complex [12], thereby producing structurally homogeneous TC9 lacking σ^{70}, which we call assembled TC9 (Fig. 2c). The assembled TC9 is also different from p-TC9 in

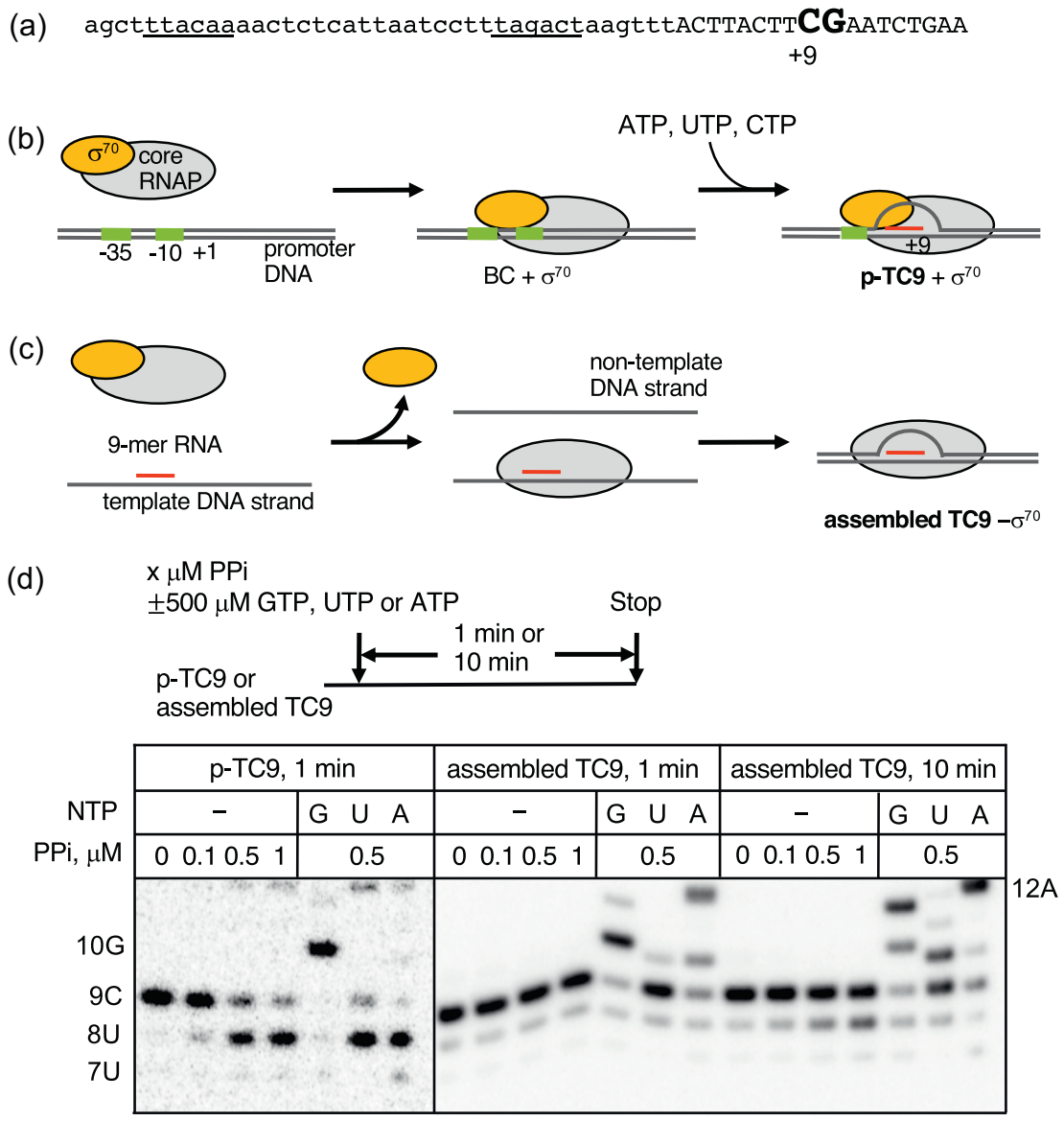

Fig. 2. Promoter-initiated TC9 (p-TC9) is much more susceptible to PPi than assembled TC9. (a) The sequence of the non-template DNA strand of the *psbA2* promoter from −38 to +18. The putative −10 and − 35 boxes are underlined, and the transcribed sequences are indicated in upper-case letters. Position +9 and + 10 are shown in the large bold letter. The transcribed sequence is modified from the intact genomic sequence. (b and c) *In vitro* production of TC9 by promoter initiation (b) and by reconstitution (c). BC represents a binary complex of RNAP and DNA. (d) *In vitro* experiments for pyrophosphorolysis and elongation of p-TC9 (left) and assembled TC9 (right). The capital letter following the number indicating RNA length represents the nature of the residue of 3′ RNA end. Reaction scheme is shown on the top of the gel.

terms of having a monophosphate at the 5′ end, while p-TC9 has a 5′ triphosphate. Both p-TC9 and the assembled TC9 complexes were purified from non-incorporated NTPs and excess oligonucleotides.

We tested p-TC9 and the assembled TC9 for their ability to add GMP or to remove 3′CMP by pyrophosphorolysis at various concentrations of PPi (Fig. 2d). Significant cleavage of the 3′ phosphodiester bond occurred in p-TC9 after 1-min incubation with 0.5 or 1 μM PPi, irrespective of how the holoenzyme was prepared (Supplementary Fig. S1). We identified CTP as the cleaved product of p-TC9 in the presence of PPi as expected from pyrophosphorolytic shortening of p-TC9 (Supplementary Fig. S2). In contrast, the assembled TC9 was highly resistant to pyrophosphorolysis even after prolonged (10 min) incubation with PPi (Fig. 2d). Notably, p-TC8, obtained from incubation of p-TC9 with PPi (Fig. 2d, the 8 U RNA), and p-TC18 (Supplementary Fig. S3) were also resistant to PPi. p-TC18 was generated from the

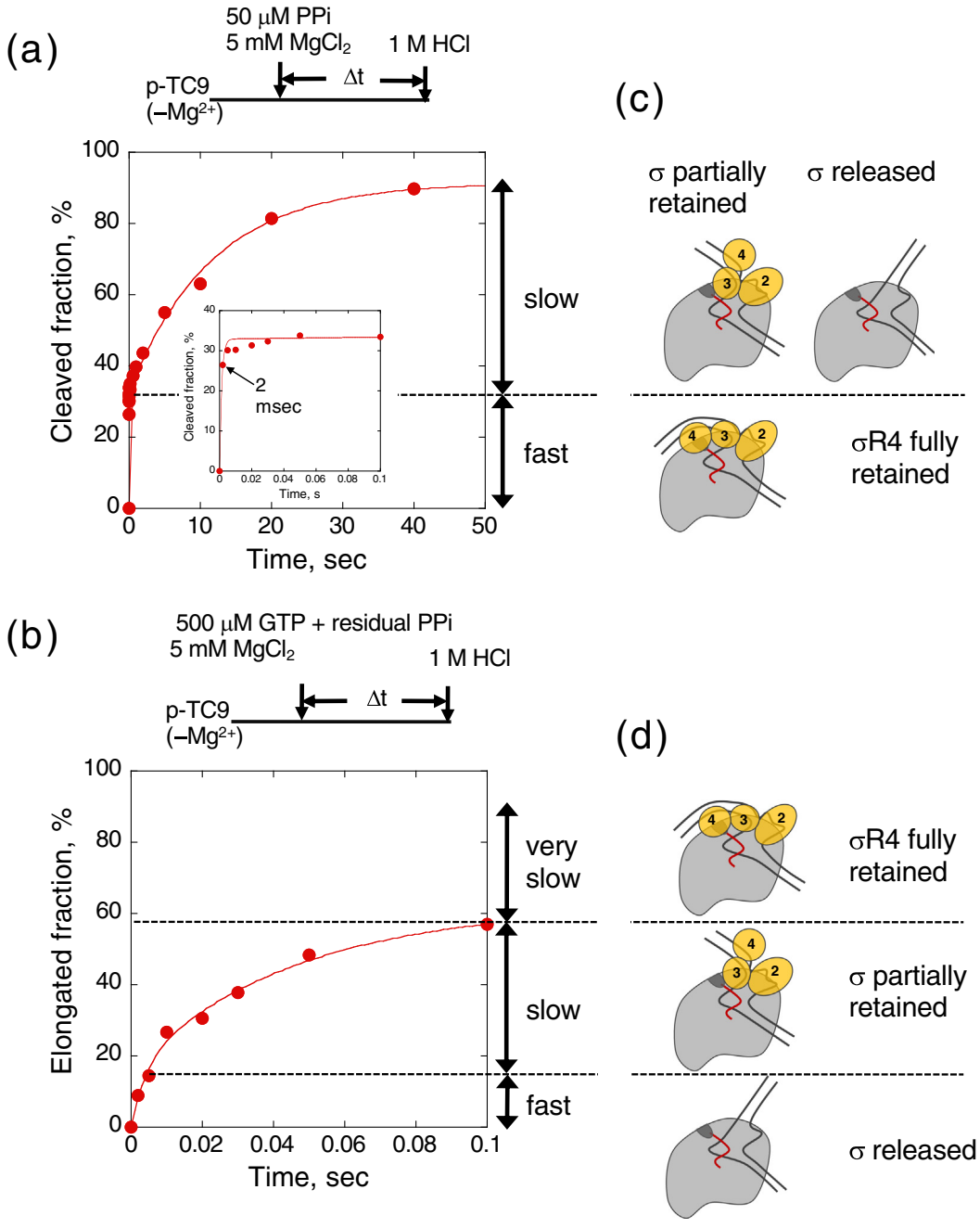

Fig. 3. Pyrophosphorolysis (a) and elongation (b) of p-TC9. Reaction scheme is shown on the top of the graph. The curves represent double-exponential fits of the data ($R^2 > 0.98$). *Y* axis represents % of the initial p-TC9. The relative abundance of each subpopulation of p-TC9 is indicated by an arrow. (c and d) Possible correlations of the three structural types (see Fig. 1) with kinetic phases observed in pyrophosphorolysis (panel c) and elongation (panel d) of p-TC9. σ^{70} region 4 is abbreviated as σR4. See Materials and Methods, and also Ref [32] for the full DNA sequence that was used for obtaining p-TC9.

same promoter in order to test the effect of the increased RNA length on pyrophosphorolysis. These results suggest that the high susceptibility of p-TC9 to PPi is unique among the TCs tested.

Both p-TC9 and the assembled TC9 fully elongated the RNA by 1 nt after 1-min incubation with 500 μM GTP (Fig. 2d). Interestingly, in the presence of 0.5 μM PPi, a significant mis-incorporation of non-cognate UMP or AMP was observed in the assembled TC9 but was not in p-TC9, indicating that the 9C was removed by pyrophosphorolysis in p-TC9 faster than mis-incorporation of UMP or AMP at 10G

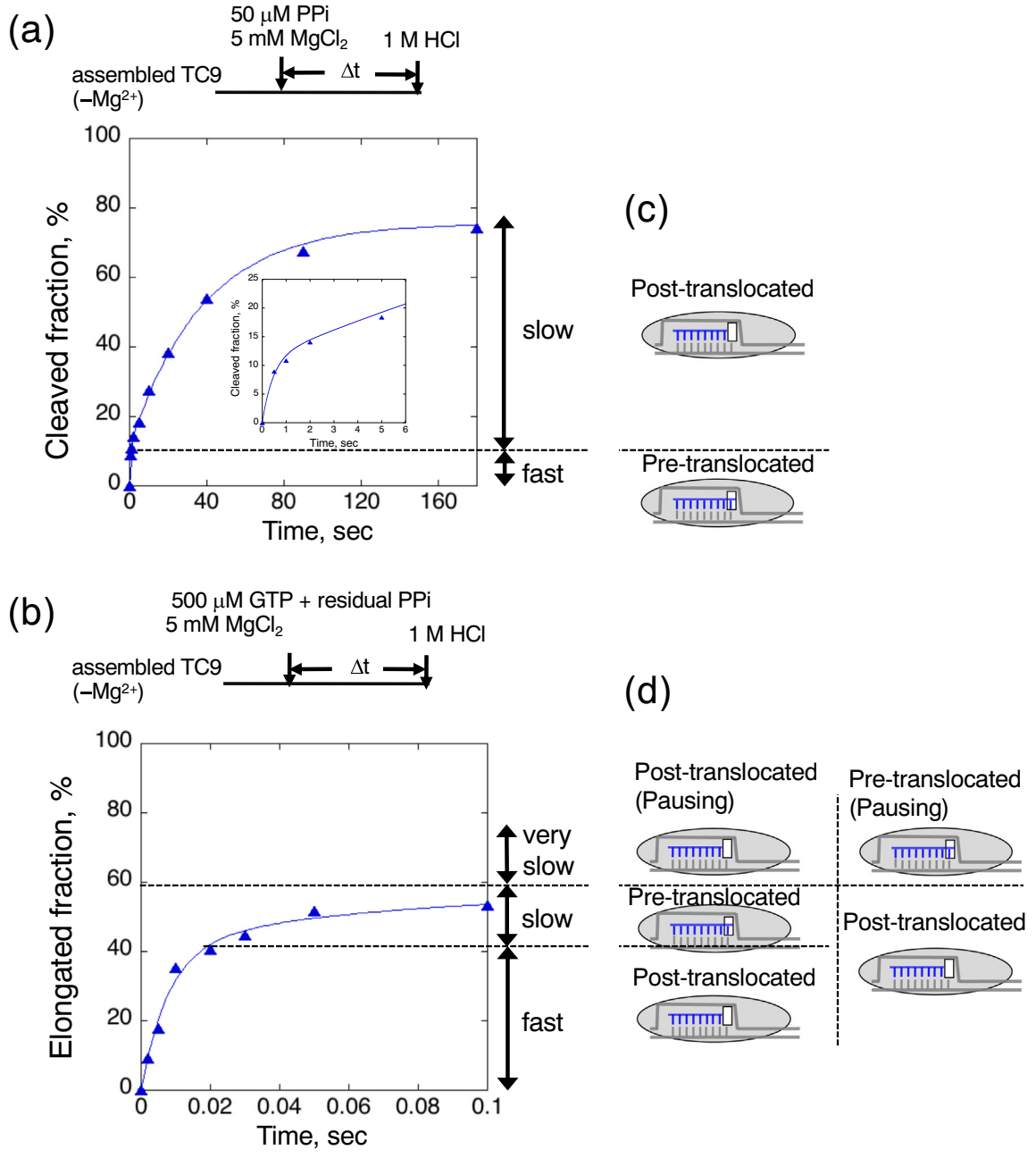

Fig. 4. Pyrophosphorolysis (a) and elongation (b) of the assembled TC9. Reaction scheme is shown on the top of the graph. The curves represent double-exponential fits of the data ($R^2 > 0.99$). *Y* axis represents % of the initial assembled TC9. The relative abundance of each subpopulation of the assembled TC9 is indicated by an arrow. (c and d) Possible correlations of the pre- and post-translocated states with kinetic phases observed in pyrophosphorolysis (panel c) and elongation (panel d) of the assembled TC9. See Materials and Methods for the DNA and RNA sequences that were used for obtaining the assembled TC.

(Fig. 2d). We analyzed further details about the effect of pyrophosphorolysis on mis-incorporation by p-TC9 (Supplementary Figs. S1, S4, and S5), which are discussed in Supplementary Text.

Next, we analyzed the kinetic homogeneity of p-TC9 and assembled TC9 by examining rapid time courses of pyrophosphorolysis and elongation in the presence of physiological concentrations of free GTP and PPi (500 and 50 μM, respectively) (Figs. 3 and 4). It has been reported that bacterial cells contain 0.5–1.5 mM of PPi in complex with biomolecules [33,34], thus [free PPi] in those cells is expected to be much lower

Table 1. The apparent rate constants ±standard errors for the fast and slow fractions (k_1 and k_2) obtained by double-exponential fitting of the data shown in Fig. 3 (p-TC9) and Fig. 4 (assembled TC9)

	Pyrophosphorolysis with 50 mM PPi		Elongation with 500 mM GTP	
	k_1 (s^{-1})	k_2 (s^{-1})	k_1 (s^{-1})	k_2 (s^{-1})
p-TC9	$(7.8 \pm 1.4) \times 10^2$	$(8.5 \pm 0.9) \times 10^{-2}$	$(2.5 \pm 1.7) \times 10^2$	$(2.2 \pm 0.5) \times 10$
assembled-TC9	2.2 ± 0.9	$(2.7 \pm 0.2) \times 10^{-2}$	$(1.3 \pm 0.3) \times 10^2$	$(2.1 \pm 1.3) \times 10$

We did not present the quantitative differences in the amplitudes of the two kinetic phases that were revealed by the fitting curves shown in Figs. 3 and 4, since the relative amplitudes of these phases should not perfectly match each other between different experimental setups. There are multiple possible reasons for these mismatches. For instance, a fraction of RNA might dissociate from RNAP during manipulation with the complexes or RNAP might partially lose activity by partial denaturation, and so on. However, all these processes do not affect our major conclusion.

and close to the level of K_m (~50 μM) for PPi-dependent enzymes [35,36]. The analysis revealed that in a ~30% fraction of p-TC9, pyrophosphorolysis was 3-fold faster than elongation in the presence of physiological concentrations of GTP and PPi (Table 1, k_1, and Fig. 3a and b). Consistent with the result shown in Fig. 2d, this PPi-sensitive fraction was not observed in the reaction by assembled TC9. In contrast, all active fractions of the assembled-TC9 were pyrophosphorolyzed at least 60-fold slower than a rapid fraction of elongation (Table 1, k_1, and Fig. 4a and b).

According to structural analysis, rapid pyrophosphorolysis requires a pre-translocated state of the complex, in which the active site is accessible to PPi, but not to NTP [37,38]. Indeed, our rapid kinetic analysis showed that the ~30% fraction of p-TC9 was very slow in GMP addition (Fig. 3a and b),

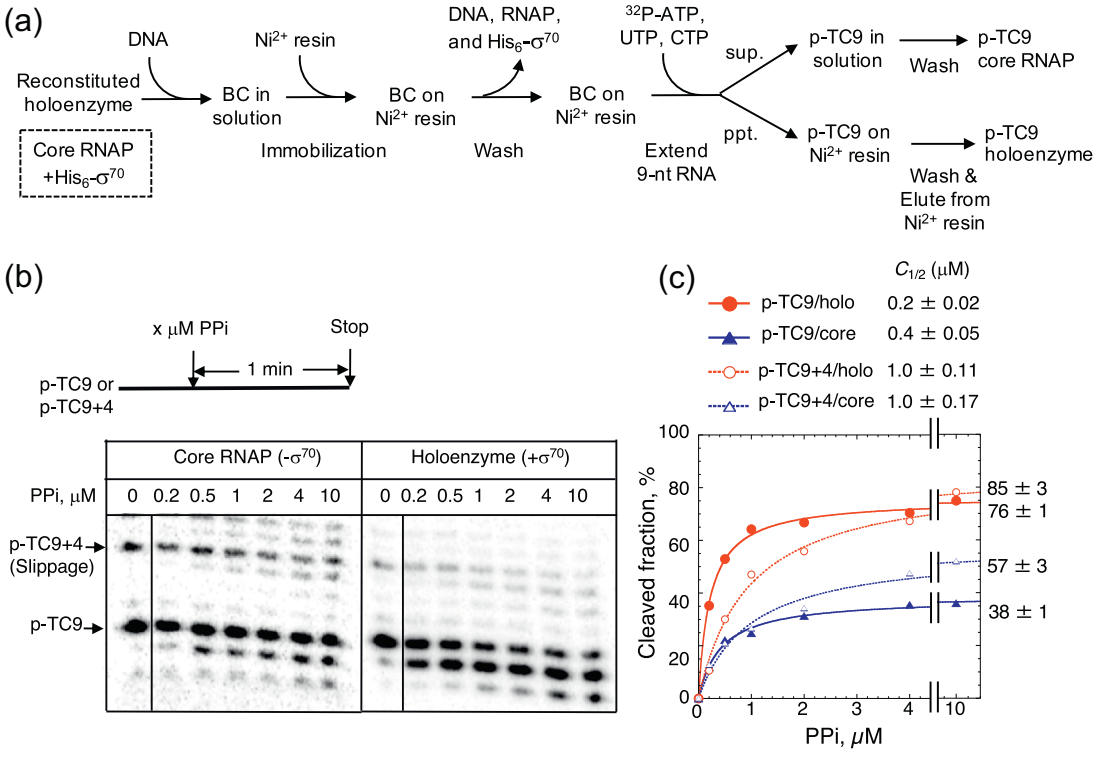

Fig. 5. Retention of σ^{70} is necessary for the enhanced pyrophosphorolysis in p-TC9. (a) The experimental method to separate p-TC9/holo (+σ^{70}) from p-TC9/core (−σ^{70}). (b) Pyrophosphorolysis by p-TC9 and the slippage product p-TC9 + 4 in the presence or absence of σ^{70} retention. Reaction scheme is shown on the top of the gel. (c) Quantitative comparison of the pyrophosphorolysis observed in panel b. The curves represent Michaelis–Menten-type hyperbolic fits of the data ($R^2 > 0.98$) shown in panel b. PPi concentrations at half saturation ($C_{1/2}$) and saturating levels of the PPi-cleaved fraction ±standard errors are shown on the top of the graph and on the right side of the graph, respectively.

which supports the presence of a substantial pre-translocated fraction of p-TC9. Due to the same ~30% fraction size, this very slow elongation fraction can be interpreted as the rapid fraction of pyrophosphorolysis. We suggest that both the very slow elongation and the rapid pyrophosphorolysis are caused by the retention of σ^{70} region 4 within p-TC9 (Fig. 3a and c). In this context, the ~60% fraction undergoing slower pyrophosphorolysis (Fig. 3a) might represent a mixture of the two complexes partially retaining σ^{70} and not retaining σ^{70} (Fig. 3c), which might also correspond to slow (~45%) and fast (~15%) elongating fractions, respectively (Fig. 3b and d). Alternatively, the ~30% very slow fraction might be a backtracked RNAP complex performing abortive initiation [39,40]. However, this possibility is unlikely, because this ~30% fraction was elongated with GTP within 1 min (Fig. 2d), which was beyond the experimental time scale (Fig. 3b). A GMP addition by an abortive synthesis is expected to be much longer than 1 min (see Discussions for further details) [39,40].

In the assembled TC9, the fractions undergoing fast and slow pyrophosphorolysis were interpreted as the fractions slow and fast (alternatively, very slow and slow + fast) in elongation, respectively (Fig. 4). There should be no σ^{70}-dependent conformational heterogeneity in the assembled TC9 lacking σ^{70}. Based on the previous rapid kinetic analysis combined with exonuclease III DNA footprinting analysis evaluating translocation equilibrium of an RNAP [3], the fractions of the assembled TC9 were interpreted as the relative abundance of pre- and post-translocated states (Fig. 4c and d). In this context, the ~18% fraction for a very slow elongation (Fig. 4b and d) may represent pausing at a post-translocated state [41] or, alternatively, a pre-translocated state [4] as shown previously.

These conformational assignments to different kinetic fractions of p-TC9 and assembled-TC9 are speculative, and hence, alternative interpretations are also possible. For instance, σ^{70} may allosterically affect structure of the active site of RNAP, making it more sensitive to PPi and less responsive to NTP. It is also possible that the slow-elongating fraction (~30%) of p-TC9 may be partially attributed to a rapid conversion of p-TC9 to p-TC8 by the PPi contaminating GTP (~1/1000; Supplementary Table S1).

σ^{70} is required for the enhanced pyrophosphorolysis in the TC with 9-nt RNA

To examine whether retention of σ^{70} was responsible for the high sensitivity of p-TC9 to PPi, we prepared p-TC9 by using native (untagged) core RNAP and hexahistidine-tagged σ^{70} (p-TC9/holo). The binary complex (BC) was obtained at the *psbA2* promoter as described in Fig. 5a followed by immobilization on Ni^{2+}-NTA agarose and incubation with ATP, CTP, and UTP to form p-TC9. The p-TC9 fraction without σ^{70} (p-TC9/core) was collected in the supernatant leaving p-TC9/holo attached to the beads. p-TC9/holo was eluted from the beads by adding imidazole (see Supplementary Fig. S6 for time course of p-TC9 release from the beads). Both p-TC9 fractions were additionally purified from NTPs, PPi, and short abortive RNA.

The major (~80%) fraction of p-TC9/holo was substantially more sensitive to PPi compared to p-TC9/core (Fig. 5b and c). Importantly, both p-TC9s were mostly elongated with 4 NTPs within 5 s (Supplementary Fig. S7). About 20% for p-TC9/core and 10% for p-TC9/holo could not elongate their RNA after an incubation for 90 s with 4 NTPs indicating the presence of a catalytically inactive fraction in both samples (Supplementary Fig. S7). This 10% inactive fraction of p-TC9/holo might derive from the moribund complex performing only slow abortive synthesis [14,18,19,42,43]. Even if that is the case, such a 10% difference in the inactive fractions cannot account for the 2-fold difference observed in the half-saturation constants for pyrophosphorolysis between p-TC9/holo and p-TC9/core ($C_{1/2}$, Fig. 5c). Thus, we concluded that p-TC9 contained little moribund complex, and retention of σ^{70} in the productive complex enhanced the pyrophosphorolysis prior to escape of the complex to elongation.

The holoenzyme used in the experiment shown in Fig. 5 was a reconstituted preparation and different from a native and non-reconstituted holoenzyme used in the experiments shown in Figs. 2–4. The difference in the elongation rate and pausing properties has been reported between such preparations [44]. We showed that such a difference within this study is limited to an increased inactive fraction in the purified core RNAP (see Supplementary Discussions and Supplementary Fig. S1A). It is also notable that the procedure to isolate p-TC9/holo from p-TC9/core may affect the population of PPi-hypersensitive intermediate (see Materials and Methods) as this procedure required a 2-fold longer incubation time than the regular procedure for p-TC9 synthesis. Thus, we have focused on comparing the half-saturation constants, which are usually considered most reliable. In any case, such a variation does not affect our qualitative conclusions about the different PPi-sensitivity of p-TC9/holo and p-TC9/core originating from one and the same holoenzyme (Fig. 5).

RNA extension beyond 9 nt eliminates the TC fraction hypersensitive to PPi

When we generated complexes expected to be p-TC9 from the *psbA2* promoter, we found other TCs with longer nascent RNAs: the major one was denoted as p-TC9 + 4 in Fig. 5b. Our interpretation of the products is reiterative transcription due to slippage between the transcript and DNA template [45,46], where AGUU transcribed from +1 to +4 on the *psbA2* promoter slips back to the AGTT template

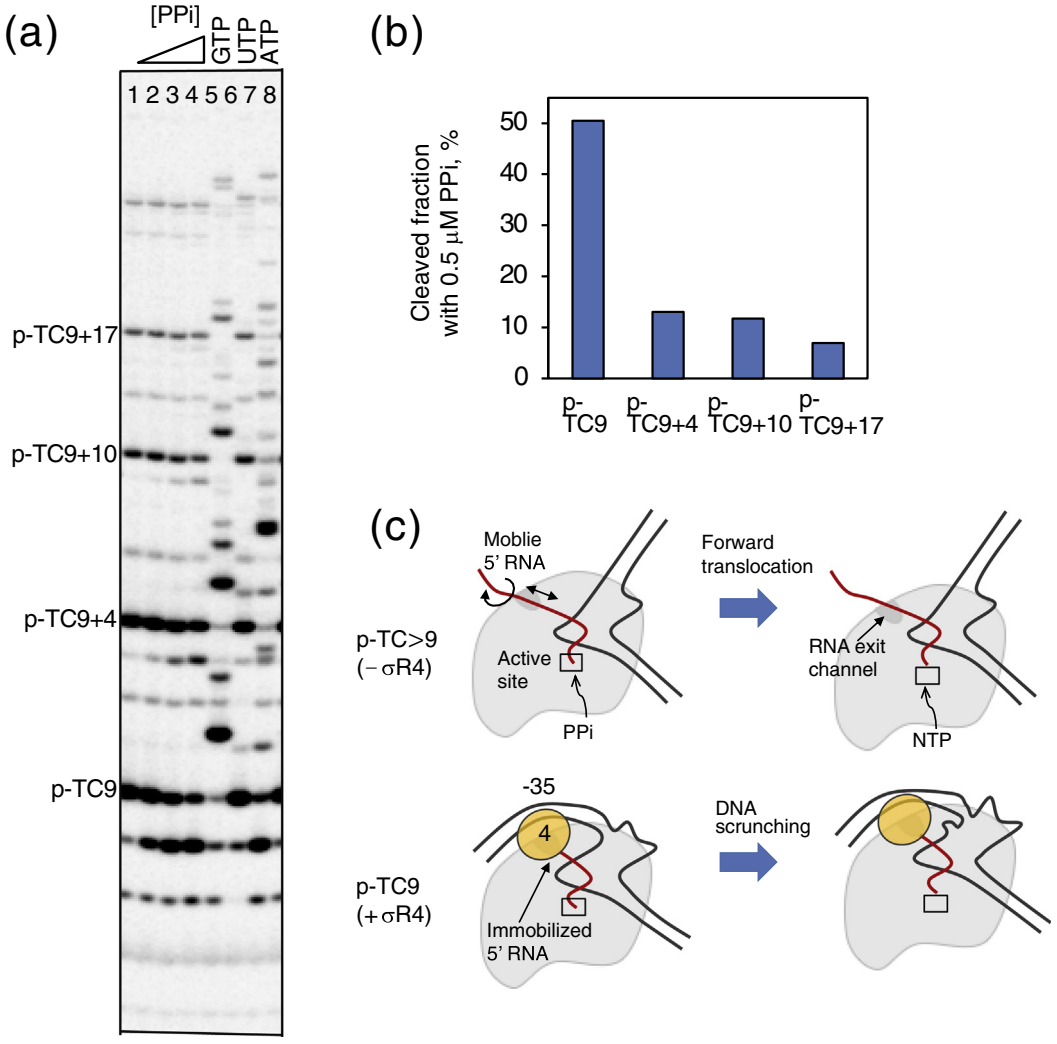

Fig. 6. The nascent RNA length affects pyrophosphorolysis and elongation. (a) Pyrophosphorolysis and elongation by p-TCs and p-TCs with >9-nt RNA (p-TC > 9 s), which were generated on the *psbA2* promoter. Lanes 1–4; 1-min incubation with buffer, 0.1 μM, 0.5 μM, or 1 μM PPi (numerical order). Lanes 5–8; 1-min incubation with GTP, UTA, or ATP of 500 μM each (numerical order). Any 500 μM NTP contains residual ~0.5 μM PPi (see Supplemental Table S1). (b) The pyrophosphorolyzed fractions observed in panel A were quantified. (c) A structural model explaining the nascent RNA that is longer than 9 nt decreases PPi susceptibility of p-TC. A fraction of p-TC9 retains σ^{70} region 4 (σR4), which limits motions of the 5′ nascent RNA (bottom). When the fraction of p-TC9 is elongated to p-TC > 9 (top), σR4 is dissociated from RNAP, allowing the increased 5′ nascent RNA motions. Pre-translocated state (left, PPi accessible) and post-translocated state (right, NTP-accessible) are schematically shown. Forward translocation to empty the active site in p-TC > 9 is replaced by DNA scrunching in p-TC9 due to the association of σR4 with DNA at −35 box. In p-TC9, the scrunching free energy is generated per forward translocation [14], causing the energetically favorable pre-translocated state and the resultant unfavorable post-translocated state.

sequence from −4 to −1, resulting in an addition of 4-nt extra RNA sequence at the 5′ end [32]. Interestingly, such a slippage product p-TC9 + 4/holo was significantly less susceptible to PPi than the original p-TC9/holo with the ~5-fold $C_{1/2}$ of p-TC9/holo (Fig. 5c). The $C_{1/2}$ values of p-TC9 + 4/holo and p-TC9 + 4/core were the same (Fig. 5c), indicating that the PPi susceptibility was also not affected by retention of σ^{70} in the presence of the extra RNA. Since the holoenzyme fraction had lower abundance of p-TC9 + 4 relative to p-TC9 when compared to the core RNAP fraction (Fig. 5b, lanes for 0 μM PPi), the extra RNA synthesis did not fully release but significantly reduced σ^{70} that was retained in RNAP. Taken together, these results indicate that not only the association of σ^{70} but also the 9-nt nascent RNA length appear crucial for determining the high sensitivity of p-TC9 to PPi.

We also found that the TCs generated by the promoter-directed transcription (p-TCs) had

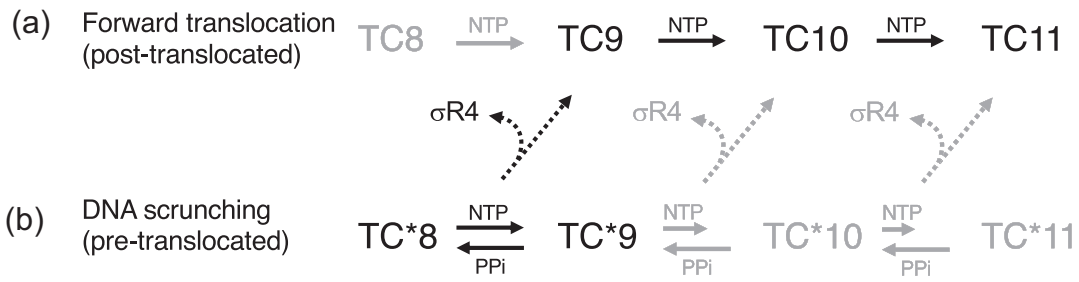

Fig. 7. The mechanistic model explaining the transition from initiation to elongation. (a) Forward translocation and the following NMP addition is not interfered without an occlusion of the 5′ nascent RNA path by σ^{70} region 4 (σR4), allowing a productive elongation from TC8 to TC11. Pyrophosphorolysis is negligible compared with elongation and thus is not shown. (b) Forward translocation is interfered by σR4 occlusion of the nascent RNA path and is replaced by DNA scrunching. Pyrophosphorolysis becomes significant because of the dominant pre-translocated state. TCs with increased susceptibility to PPi are generated with progress in DNA scrunching, which are denoted as TC*. During numerous exchanges between TC*8 and TC*9, σR4 is occasionally displaced from TC*8 to form TC9 leading to productive elongation (i.e., a shift from the pathway shown in panel b to the corresponding pathway shown in panel a). TCs*≥9 rarely elongate RNA because the longer the nascent RNA is, the more the scrunching free energy is generated (i.e., the more unfavorable the NTP-accessible post-translocated state is) [14]. The predicted pathways without any supports by experimental data are indicated by gray letters and arrows.

decreasing sensitivity to PPi as the nascent RNA was elongated from 9-nt to 13-nt, 21-nt and 26-nt, while the ability to elongate the RNA with GTP is retained (Fig. 6a and b, p-TC9 + 4, p-TC9 + 10, and p-TC9 + 17). This result shows that elongation of the nascent RNA beyond 9 nt inhibited the high pyrophosphorolytic activity of p-TC9. Any p-TCs with RNAs exceeding 9-nt length were elongated with the substrate preference in the order of GTP, ATP, and UTP, indicating that those p-TCs shared the same template sequence at the active site, as expected from the slippage [45,46]. However, the patterns of elongation with ATP showed a distinct difference between p-TC 9 and p-TC≥9 + 4 (Fig. 6a, lane 8). This difference may be related to the sequence-specific pausing identified previously [6] in addition to the nascent RNA length and σ^{70} association. We discussed this issue in Supplementary Text.

Discussion

A structural model of the enhanced pyrophosphorolysis

We demonstrated that pyrophosphorolysis is enhanced by σ^{70} retention in TC and that this hypersensitivity to PPi is observed only in the TC with a 9-nt-long nascent RNA. This observation can be interpreted by using the currently available x-ray crystal structures of the transcription initiation complexes at various reaction stages [23–26] as well as the results of a fluorescence resonance energy transfer experiment [29]. TC9 is here found to be structurally heterogeneous, and the nascent RNA is interpreted to be too short to expel its 5′-end from the RNA exit channel by releasing σ^{70} region 4 from the −35 segment through all fractions of TC9. Only in the TCs with RNA longer than 9 nt, the RNA 5′ end is considered to be expelled from the inside of TC (Figs. 1 and 6c). The σ^{70} region 4 also induces DNA scrunching because RNAP remains bound to the promoter DNA at the −35 box by the region 4 [29], and hence, its displacement from RNAP enables forward translocation of the enzyme without the scrunching (Fig. 6c). In other words, the enhanced pyrophosphorolysis has two distinct mechanistic aspects: first, interaction (or immobilization) of the 5′ end of the nascent RNA with σ^{70} region 4 and, second, DNA-scrunching-dependent conformational and energetic changes in the TC.

The first aspect of the model is supported by the observation that σ^{70} region 4 occludes the path for the nascent RNA when it becomes longer than ~9-nt [47]. The σ^{70} region 4 contains a basic patch that can further strengthen its interaction with the 5′ triphosphate [48]. Indeed, the interaction of σ^{70} 3.2 loop with the 5′ triphosphate of the shorter (4- to 6-nt) nascent RNA has been revealed in the crystal structure of the *E. coli* initiation complex [25,47], and its role for promoter escape has been also suggested by a more recent study [39,49]. The difference in PPi susceptibility observed between p-TC9 and the assembled TC9 (Fig. 2d) might be related to the absence of the 5′ triphosphate in the assembled TC9. During the forward translocation of TCs with σ^{70}, 1-base-pair DNA is scrunched into RNAP complex with DNA distortion, which makes the resultant post-translocated complex less energetically favorable than the regular translocation of TCs without σ^{70} (Fig. 6c) [14,29]. This energetics supports the second aspect of the model. Therefore, the TC that involves DNA scrunching should be

more susceptible to PPi because of the relatively favorable pre-translocated state, which is required for pyrophosphorolysis.

Possible biological significance of the enhanced pyrophosphorolysis

In this study, we showed that during the initiation-to-elongation transition, at least one TC, TC9, has a fraction exhibiting unusually high pyrophosphorolytic rate exceeding the typical rate of phosphodiester bond formation at physiological concentrations of PPi and NTP. Therefore, when NTPs and PPi are present, TC9 and the pyrophosphorolyzed product TC8 are rapidly and iteratively converted between each other. Since this is a kind of reverse reaction and might be disadvantageous, what is its biological significance? We here propose a mechanistic model in which multiple TC8-to-TC9 interconversions are essential to keep TCs on the right track of promoter escape accompanied by the complete displacement of σ^{70} region 4 (and 3.2 loop) to clear the RNA exit channel (Fig. 7a and b). The PPi-sensitive complex stochastically but inevitably exists in a promoter-directed transcription. This complex is unstable probably because of its structural distortion accompanied with the exit channel blocked by σ^{70} region 4, leading to preferential pyrophosphorolysis rather than elongation. In other words, the displacement of σ^{70} region 4 prevents pausing or arrest during initiation caused by the energetically unfavorable forward translocation via DNA scrunching.

Accordingly, we also propose that TC8 and TC9 containing σ^{70} (Fig. 7b, TC*8 and TC*9) stochastically displace σ^{70} region 4 (and 3.2 loop) by itself during the repetitive TC*8-to-TC*9 interconversions. In this model, TC*9 decreases in a timescale necessary for preventing promoter arrest in physiological conditions (Fig. 7b and Supplementary Discussions): the timescale of TC*9-to-TC10 transition eliminating the association of σ^{70} region 4 is likely to be similar to that of TC*9-to-TC*10 elongation retaining σ^{70}. In other words, the rapid pyrophosphorolysis is a step necessary for converting the σ^{70}-associated TC*9 into TC10 and more mature elongation complexes lacking σ^{70}. Occlusion of the nascent RNA path by σ^{70} region 4 may cause the promoter-proximal arrest [50].

The rapid pyrophosphorolysis of the initiation-to-elongation intermediate has not been attracted. One of the reasons is that NTPs are generally contaminated with PPi (Supplementary Table S1), and pyrophosphorolysis unintentionally occurred in experiments using high concentrations of NTPs, canceling the existing effects of exogenous PPi. Our preparation and storage of p-TCs were careful to avoid such cancelation (see Supplementary Discussions and Supplementary Fig. S8).

It has been suggested that the σ dissociation is caused by a steric clash between σ region 3.2 loop and the elongating abortive RNA [24,51]. Although the previously proposed mechanism can explain the abortive synthesis by a moribund complex, such an abortive synthesis does not lead to productive elongation [14,18,19,42,43,49], being unable to accelerate the promoter escape. We emphasize that our model based on the rapid and reversible exchanges of TCs with 9 and 8 nt RNAs under DNA scrunching is attributed to the productive complex but not moribund complex; these two different complexes that are formed in initiation are sometimes confused. Multiple lines of experimental evidence suggest that the holoenzyme of the moribund complex backtracks along DNA rather than involving DNA scrunching for releasing abortive RNA [14,17,39,40]. During backtracking, the active site is inaccessible to accept either NTP or PPi. Thus, the abortive RNA synthesis by the moribund complex will be much slower (usually, up to 20 min [43]) than milliseconds-timescale exchanges observed between TC9 and TC8, and iteratively produce shorter products usually from 2 to ~8 nt. It is also notable that the conversion of the moribund complex to the productive complex without binding of a relevant transcription factor is unlikely because of the presence of an intrinsically high-energy barrier between them [17,18]. Therefore, the contribution of moribund complex in the pyrophosphorolysis is small, if any, within the timescales of our observation, that is, a few milliseconds to several tens of seconds (see Results and Supplementary Fig. S7). In summary, this study presents the mechanism of promoter escape by the productive complex in the context of branched initiation pathway of bacterial transcription. A checkpoint mechanism that directs RNAP to productive elongation has been previously proposed [49], and our study specifies multiple cycles of try-and-error mechanism, namely, cleavage and re-synthesis of the 3′ phosphodiester bond of the 9-nt RNA.

The highly reversible bond formation during the initiation-to-elongation transition might play a key role in maintaining genomic integrity in bacteria. During the initial stage of elongation, RNAP frequently falls into paused states [50,52,53], which is further stabilized by backtracking of RNAP leading to transcription arrest [54]. Interestingly, a recent genetic study revealed that collisions between replicating DNA polymerases and promoter-arrested RNAPs lead to an elevated level of DNA mutations in promoter-proximal regions of genes [55]. Retention of σ^{70} leads to the enhanced promoter-proximal pausing [56]. It is likely that the rapid pyrophosphorolysis observed in our study is essential for the efficient promoter escape, preventing RNAP accumulation at the promoter-proximal regions and toxic collisions with the replication machinery.

Materials and Methods

Reagents

NTPs and oligonucleotides were purchased from GE Healthcare and Integrated DNA Technologies, respectively. Residual concentrations of PPi in all NTP solutions were measured as approximately 3 orders of magnitude smaller concentrations of NTPs used (e.g., ~0.5 μM PPi exits in 500 μM NTP solution) by EnzCheck Pyrophosphate assay kit (Thermo Fisher Scientific), according to the manufacturer's method (Supplementary Table S1).

Purification of RNAP

E. coli RNAP carrying the hexahistidine-tag at the C-terminus of the β′ subunit was purified according to the original protocol [57]. *E. coli* cells (strain RL916) were grown in 700 mL of LB to OD600 0.8–1 and were collected by a 15-min centrifugation at 5400 *g*. All the subsequent steps were performed at 4 °C. Approximately 1 g of cells was re-suspended in 25 ml of lysis buffer 1 [300 mM Tris-acetate (pH 7.9), 100 mM potassium acetate, 10 mM $MgCl_2$, 1 mM EDTA, and 4 mM 2-mercaptoethanol]. The cells were broken by sonication, and the lysate was clarified by a 35-min centrifugation at 21,000 *g*. Imidazole (1 M; pH 7.9) was added to the supernatant to achieve 10 mM final concentration, and solid KCl was added to 1 M final concentration. The solution was loaded at 1 ml/min to a 1 ml HisTrap HP column (GE Healthcare) prewashed with 10 ml of lysis buffer 1 using the AKTA 900 Purifier (GE Healthcare) system. Then the column was washed with 20 ml of lysis buffer containing 1 M KCl and with 20 ml of Ni buffer [20 mM Tris–HCl, 5 mM $MgCl_2$, 150 mM KCl, 4 mM 2-mercaptoethanol, and 1 mM phenylmethylsulfonyl fluoride (PMSF)] containing 150 mM KCl. RNAP was eluted with a 20-ml linear gradient from 0 to 200 mM imidazole in Ni buffer. Combined fractions containing RNAP (3–4 ml) are diluted 2-fold with heparin buffer [20 mM Tris–HCl (pH 7.9), 5% glycerol, 0.5 mM EDTA, 1 mM dithiothreitol (DTT), 4 mM 2-mercaptoethanol, and 1 mM PMSF], and loaded to a 1-ml Heparin HiTrap HP (GE Healthcare). The column was washed with 15 ml of heparin buffer containing 300 mM NaCl, and RNAP was eluted with a 20-mL linear gradient from 300 to 1000 mM of NaCl in heparin buffer. Combined fractions containing RNAP (2 ml) were diluted 5-fold with Mono Q buffer [40 mM Tris–HCl (pH 8.3), 5% glycerol, 5 mM $MgCl_2$, 1 mM DTT, and 1 mM PMSF] and loaded to a Mono Q 5/50 column (GE Healthcare). The column was washed with 15 ml of Mono Q buffer containing 200 mM NaCl, and RNAP was eluted with a 25-ml linear gradient from 200 to 500 mM NaCl in Mono Q buffer. RNAP core enzyme was eluted at around 350 mM NaCl, and the RNAP holoenzyme peak closely followed the core enzyme peak. For protein storage, NaCl and glycerol were added to the protein solution at the final concentrations of 200 mM and 30%, respectively, which was frozen in aliquots in liquid nitrogen, and stored at −80 °C. The typical yield was ~350 μg of RNAP core enzyme and ~200 μg of RNAP holoenzyme from ~1 g of cells.

Purification of non-tagged RNAP

E. coli cell lysate of *E. coli* (strains MC4100 or DJ138) was obtained as described for the hexahistidine-tagged RNAP, except that ~1 g of cells was resuspended in 25 ml of lysis buffer 2 [50 mM Tris–HCl (pH 8.0), 300 mM NaCl, 10 mM $MgCl_2$, 10 mM EDTA, 1 mM DTT, 5% glycerol, and 0.2% sodium deoxycholate]. Eight percent Polymin-P solution (0.7 ml; pH 7.9) was slowly added to 22 ml of the lysate with continuous stirring on ice to achieve 0.25% final concentration of Polymin-P (modified from Refs. [57, 58]). The precipitate was collected at 5000*g* for 15 min and was resuspended in 25–30 ml of heparin buffer containing 450 mM NaCl. Polymin-P precipitate was repeatedly washed with heparin buffer containing 450 mM NaCl (typically 4–6 times) until the resulting supernatant contains no detectable protein. RNAP was eluted from the pellet by 20–25 ml of heparin buffer containing 1 M NaCl and separated from the pellet by centrifugation 8000 *g* for 30 min. The remaining pellet was resuspended in another 20–25 ml aliquot of heparin buffer containing 1 M NaCl and centrifuged again. The eluates were combined, and RNAP was precipitated by addition of ammonium sulfate to 60% saturation. The pellet was dissolved in heparin buffer and loaded to heparin column and then to Mono Q column as described above. The protein solution was frozen and stored at −80 °C as described above.

Purification of σ^{70}

E. coli cells (strain AD19275 or DJ420) were grown in 700 ml of LB medium to OD600 of 0.5–0.7. IPTG was added to 1 mM final concentration, and the culture was incubated at 30 °C for additional 3–4 h [59]. The cells were collected by a 15-min centrifugation at 5400 *g*. All the subsequent steps were performed at 4 °C. Approximately 2 g of cells was suspended in 80 ml of lysis buffer 1 [300 mM Tris-acetate (pH 7.9), 100 mM potassium acetate, 10 mM $MgCl_2$, 1 mM EDTA, and 4 mM 2-mercaptoethanol)]. The cells were broken by sonication, and the lysate was clarified by a 35-min centrifugation at 21,000 *g*. Imidazole (1 M; pH 7.9) was added to the supernatant to achieve 10 mM final concentration, and then solid KCl was added to achieve 1 M final concentration. The lysate was loaded at 2 ml/min to a 5 ml HisTrap FF column (GE Healthcare). Then the column was washed with 120 ml of lysis buffer containing 1 M KCl and with 75 ml of Ni buffer [20 mM Tris–HCl (pH 8.0), 5 mM

$MgCl_2$, 150 mM KCl, 4 mM 2-mercaptoethanol, and 1 mM PMSF]. σ^{70} was eluted at 1 ml/min with a 75-ml linear gradient of imidazole from 0 to 300 mM in Ni buffer. Fractions containing σ^{70} were combined and were loaded to Superdex 200 prep grade HiLoad 16/600 column (GE Healthcare) equilibrated with 20 mM Tris–HCl (pH 7.9), 500 mM KCl, 4 mM 2-mercaptoethanol, and 1 mM PMSF. The size exclusion chromatography was repeated two more times. The total yield of σ^{70} was about 10–15 mg, and the purity was ~90%. No RNAP subunits were detected in the final preparation of σ^{70}.

Preparation of p-TC

Promoter-initiated TC with 5′-labeled 9-nt RNA on the *psbA2* promoter was generated as described previously [32]. Briefly, to form the BC, 5–10 pmol of *E. coli* RNAP holoenzyme was mixed with 2 pmol linear DNA template (purified PCR product) containing the *psbA2* promoter (228 base pairs: −127 to +101, where +1 is a transcription start site) in 10 μl volume of transcription buffer [TB; 20 mM Tris–HCl (pH 7.9), 5 mM $MgCl_2$, 1 mM 2-mercaptoehanol, 0.1 M KCl, and 0.1 mg/ml bovine serum albumin] and incubated for 10 min at 37 °C. In order to form TC with 9-nt RNA, 5 μM ATP including [γ-^{32}P] ATP as well as 50 μM each of CTP and UTP in 10 μl volume of TB was added to the BC and incubated for 5 min at 37 °C. The TC was purified from the substrates including [γ-^{32}P] ATP as well as PPi and abortive transcripts that were released from the complexes by ultrafiltration through a 100-kDa cutoff membrane (Microcon YM-100; Millipore) [13]. In particular, the TC in 300 μl TB was concentrated to 10–15 μl by a 20-min centrifugation at 14,000 *g*. We repeated this procedure three times by adding TB to the concentrated sample. Previous our studies revealed that the concentration of the residual non-incorporated NTPs after ultrafiltration should be below the limit to be incorporated into the nascent RNA by RNAP [9,13]. The purified TC was used for experiments by dilution of the sample with TB (typically ~10 fold).

Preparation of the assembled TC9

The assembled TC9 was generated by using 5′-labeled 9-nt RNA 5′ACUUACUUC3′, template DNA strand 5′CCTTATGTATTTGTCGATGTTCAGATTCGAAGTAAGTAAACTTAGTCTAAAGGATTA3′ and non-template DNA strand 5′TAATCCTTTAGACTAAGTTTACTTACTTCGAATCTGAACATCGACAAATACATAAGGAAT3′ as described previously [60]. Briefly, 5–10 pmol of *E. coli* RNAP holoenzyme was incubated with 7.5–15 pmol of the preannealed RNA–DNA hybrid in 25–50 ml volume of TB for 10 min at room temperature. Next, 15–50 pmol of the nontemplate DNA strand was added for 10 min. The assembled TC9 was incubated with TB containing 1 M KCl for 10 min and was purified from excess RNA and DNA oligonucleotides (these can be also dissociated from RNAP during the incubation with 1 M KCl) by ultrafiltration as described above. The purified assembled TC9 was used for experiments by dilution of the sample with TB (typically ~10 fold).

Separation of p-TC9 in the presence or absence of σ^{70}

In order to reconstitute holoenzyme, 5–10 pmol each of native core enzyme and hexahistidine-tagged σ^{70} protein was mixed and incubated for 5 min at 37 °C. The BC with the linear DNA template was formed as described above, and then was immobilized on Ni^{2+}-NTA agarose (Qiagen) in TB as described previously [61]. The immobilized BC was washed intensively with TB on Ni^{2+}-NTA agarose. p-TC9 was formed as describe above, with a difference in the incubation time of 10 min, during which TC9 that was detached from σ^{70} upon 9-nt RNA synthesis was released into the supernatant of the resin. The released p-TC9 was then collected in a test tube. TC9 with σ^{70} that was immobilized on the resin was washed with TB and then was eluted from the resin by adding 100 mM imidazole as described previously [62]. Each of the TC9s (with or without σ^{70}) was purified from NTPs and PPi as well as abortive transcripts by passing through MicroSpin G50 column (GE Healthcare) equilibrated with TB. We also described the time course of this procedure in Supplementary Fig. S6.

In vitro transcription

Details about the experimental setups are described in the corresponding main figures or supplementary figures. All reactions were performed in TB at 37 °C. Reactions were stopped by gel-loading buffer (5 M urea and 25 mM EDTA at final concentrations). Any reactions for shorter than 5 s were performed using RQF3 rapid quench-flow instrument (KinTek Corporation) and were quenched by 1 M HCl, as described previously [62]. In the rapid quench-flow measurement, TC9 in TB without $MgCl_2$ was mixed with equal volume of TB containing 10 mM $MgCl_2$ and 100 μM PPi (for pyrophosphorolysis) or TB containing 10 mM $MgCl_2$ and 1 mM GTP (for elongation). RNA products were analyzed by polyacrylamide gel electrophoresis using a 20% gel containing 7 M urea.

All the experiments with presented results in this study were repeated two or more times, and the represented ones are shown.

Acknowledgments

We thank Donald L. Court and Koh Takeuchi for critical reading of the manuscript. This work was

financially supported by the Intramural Research Program of the National Institutes of Health/National Cancer Institute (to M.K.), by the Sasakawa Scientific Research Grant (to M.I.), by the Leave a Nest Scientific Research Grant (to M.I.), and by JSPS KAKENHI Grant Number 18 K18731 (to M.I.).

Appendix A. Supplementary data

Supplementary data to this article can be found online at https://doi.org/10.1016/j.jmb.2019.04.020.

Received 8 January 2019;
Received in revised form 13 April 2019;
Accepted 15 April 2019
Available online 26 April 2019

Keywords:
pyrophosphate;
sigma subunit;
RNA polymerase;
branched initiation pathway;
productive complex

[4]Present address: Advanced Development Center, Horiba Ltd., Kyoto, 601-8510, Japan.

Abbreviations used:
nt, nucleotide; NTP, ribonucleoside triphosphate; PPi, pyrophosphate; RNAP, RNA polymerase; TC, ternary complex; BC, binary complex.

References

[1] A. Kornberg, Active center of DNA polymerase, Science. 163 (1969) 1410–1418.
[2] V.S. Anand, S.S. Patel, Transient state kinetics of transcription elongation by T7 RNA polymerase, J. Biol. Chem. 281 (2006) 35677–35685.
[3] C.L. Vitiello, M.L. Kireeva, L. Lubkowska, M. Kashlev, M. Gottesman, Coliphage HK022 Nun protein inhibits RNA polymerase translocation, Proc. Natl. Acad. Sci. U. S. A. 111 (2014) E2368–E2375.
[4] M. Imashimizu, M.L. Kireeva, L. Lubkowska, D. Gotte, A.R. Parks, J.N. Strathern, et al., Intrinsic translocation barrier as an initial step in pausing by RNA polymerase II, J. Mol. Biol. 425 (2013) 697–712.
[5] P.P. Hein, M. Palangat, R. Landick, RNA transcript 3′-proximal sequence affects translocation bias of RNA polymerase, Biochemistry. 50 (2011) 7002–7014.
[6] M. Imashimizu, H. Takahashi, T. Oshima, C. McIntosh, M. Bubunenko, D.L. Court, et al., Visualizing translocation dynamics and nascent transcript errors in paused RNA polymerases in vivo, Genome Biol. 16 (2015) 98.
[7] T.A. Rozovskaya, A.A. Chenchik, R. Beabealashvilli, Processive pyrophosphorolysis of RNA by *Escherichia coli* RNA polymerase, FEBS Lett. 137 (1982) 100–104.
[8] S.C. Hung, M.E. Gottesman, The Nun protein of bacteriophage HK022 inhibits translocation of *Escherichia coli* RNA polymerase without abolishing its catalytic activities, Genes Dev. 11 (1997) 2670–2678.
[9] M.L. Kireeva, C. Trang, G. Matevosyan, J. Turek-Herman, V. Chasov, L. Lubkowska, et al., RNA–DNA and DNA–DNA base-pairing at the upstream edge of the transcription bubble regulate translocation of RNA polymerase and transcription rate, Nucleic Acids Res. 46 (2018) 5764–5775.
[10] M. Righini, A. Lee, C. Canari-Chumpitaz, T. Lionberger, R. Gabizon, Y. Coello, et al., Full molecular trajectories of RNA polymerase at single base-pair resolution, Proc. Natl. Acad. Sci. U. S. A. 115 (2018) 1286–1291.
[11] N. Komissarova, M.L. Kireeva, J. Becker, I. Sidorenkov, M. Kashlev, Engineering of elongation complexes of bacterial and yeast RNA polymerases, Methods Enzymol. 371 (2003) 233–251.
[12] I. Sidorenkov, N. Komissarova, M. Kashlev, Crucial role of the RNA:DNA hybrid in the processivity of transcription, Mol. Cell 2 (1998) 55–64.
[13] M. Kireeva, Y.A. Nedialkov, X.Q. Gong, C. Zhang, Y. Xiong, W. Moon, et al., Millisecond phase kinetic analysis of elongation catalyzed by human, yeast, and *Escherichia coli* RNA polymerase, Methods. 48 (2009) 333–345.
[14] K.L. Henderson, L.C. Felth, C.M. Molzahn, I. Shkel, S. Wang, M. Chhabra, et al., Mechanism of transcription initiation and promoter escape by *E. coli* RNA polymerase, Proc. Natl. Acad. Sci. U. S. A. 114 (2017) E3032-E40.
[15] I. Petushkov, D. Esyunina, V. Mekler, K. Severinov, D. Pupov, A. Kulbachinskiy, Interplay between sigma region 3.2 and secondary channel factors during promoter escape by bacterial RNA polymerase, Biochem. J. 474 (2017) 4053–4064.
[16] N. Shimamoto, T. Kamigochi, H. Utiyama, Release of the sigma subunit of *Escherichia coli* DNA-dependent RNA polymerase depends mainly on time elapsed after the start of initiation, not on length of product RNA, J. Biol. Chem. 261 (1986) 11859–11865.
[17] N. Shimamoto, Nanobiology of RNA polymerase: biological consequence of inhomogeneity in reactant, Chem. Rev. 113 (2013) 8400–8422.
[18] T. Kubori, N. Shimamoto, A branched pathway in the early stage of transcription by *Escherichia coli* RNA polymerase, J. Mol. Biol. 256 (1996) 449–457.
[19] M. Susa, T. Kubori, N. Shimamoto, A pathway branching in transcription initiation in *Escherichia coli*, Mol. Microbiol. 59 (2006) 1807–1817.
[20] B.E. Nickels, S.J. Garrity, V. Mekler, L. Minakhin, K. Severinov, R.H. Ebright, et al., The interaction between sigma70 and the beta-flap of *Escherichia coli* RNA polymerase inhibits extension of nascent RNA during early elongation, Proc. Natl. Acad. Sci. U. S. A. 102 (2005) 4488–4493.
[21] N. Komissarova, M. Kashlev, Functional topography of nascent RNA in elongation intermediates of RNA polymerase, Proc. Natl. Acad. Sci. U. S. A. 95 (1998) 14699–14704.
[22] S. Borukhov, E. Nudler, RNA polymerase holoenzyme: structure, function and biological implications, Curr. Opin. Microbiol. 6 (2003) 93–100.
[23] K.S. Murakami, S.A. Darst, Bacterial RNA polymerases: the wholo story, Curr. Opin. Struct. Biol. 13 (2003) 31–39.
[24] K.S. Murakami, S. Masuda, S.A. Darst, Structural basis of transcription initiation: RNA polymerase holoenzyme at 4 Å resolution, Science. 296 (2002) 1280–1284.
[25] Y. Zuo, T.A. Steitz, Crystal structures of the *E. coli* transcription initiation complexes with a complete bubble, Mol. Cell 58 (2015) 534–540.

[26] Y. Zhang, Y. Feng, S. Chatterjee, S. Tuske, M.X. Ho, E. Arnold, et al., Structural basis of transcription initiation, Science. 338 (2012) 1076–1080.
[27] A. Feklistov, B.D. Sharon, S.A. Darst, C.A. Gross, Bacterial sigma factors: a historical, structural, and genomic perspective, Annu. Rev. Microbiol. 68 (2014) 357–376.
[28] P. Deighan, C. Pukhrambam, B.E. Nickels, A. Hochschild, Initial transcribed region sequences influence the composition and functional properties of the bacterial elongation complex, Genes Dev. 25 (2011) 77–88.
[29] A.N. Kapanidis, E. Margeat, S.O. Ho, E. Kortkhonjia, S. Weiss, R.H. Ebright, Initial transcription by RNA polymerase proceeds through a DNA-scrunching mechanism, Science. 314 (2006) 1144–1147.
[30] A. Revyakin, C. Liu, R.H. Ebright, T.R. Strick, Abortive initiation and productive initiation by RNA polymerase involve DNA scrunching, Science. 314 (2006) 1139–1143.
[31] B. Liu, Y. Zuo, T.A. Steitz, Structures of *E. coli* sigmaS-transcription initiation complexes provide new insights into polymerase mechanism, Proc. Natl. Acad. Sci. U. S. A. 113 (2016) 4051–4056.
[32] M. Imashimizu, K. Tanaka, N. Shimamoto, Comparative study of cyanobacterial and *E. coli* RNA polymerases: misincorporation, abortive transcription, and dependence on divalent cations, Genet. Res. Int. 2011 (2011).
[33] E. Kukko-Kalske, M. Lintunen, M.K. Inen, R. Lahti, J. Heinonen, Intracellular PPi concentration is not directly dependent on amount of inorganic pyrophosphatase in *Escherichia coli* K-12 cells, J. Bacteriol. 171 (1989) 4498–4500.
[34] E. Kukko, J. Heinonen, The intracellular concentration of pyrophosphate in the batch culture of *Escherichia coli*, Eur. J. Biochem. 127 (1982) 347–349.
[35] A.S. Reshetnikov, O.N. Rozova, V.N. Khmelenina, I.I. Mustakhimov, A.P. Beschastny, J.C. Murrell, et al., Characterization of the pyrophosphate-dependent 6-phosphofructokinase from *Methylococcus capsulatus* Bath, FEMS Microbiol. Lett. 288 (2008) 202–210.
[36] I. Bruchhaus, T. Jacobs, M. Denart, E. Tannich, Pyrophosphate-dependent phosphofructokinase of *Entamoeba histolytica*: molecular cloning, recombinant expression and inhibition by pyrophosphate analogues, Biochem. J. 316 (1996) 57–63 Pt 1.
[37] F. Brueckner, J. Ortiz, P. Cramer, A movie of the RNA polymerase nucleotide addition cycle, Curr. Opin. Struct. Biol. 19 (2009) 294–299.
[38] M. Kireeva, M. Kashlev, Z.F. Burton, Translocation by multi-subunit RNA polymerases, Biochim. Biophys. Acta 1799 (2010) 389–401.
[39] E. Lerner, S. Chung, B.L. Allen, S. Wang, J. Lee, S.W. Lu, et al., Backtracked and paused transcription initiation intermediate of *Escherichia coli* RNA polymerase, Proc. Natl. Acad. Sci. U. S. A. 113 (2016) E6562-E71.
[40] D. Duchi, D.L. Bauer, L. Fernandez, G. Evans, N. Robb, L.C. Hwang, et al., RNA polymerase pausing during initial transcription, Mol. Cell 63 (2016) 939–950.
[41] M.L. Kireeva, M. Kashlev, Mechanism of sequence-specific pausing of bacterial RNA polymerase, Proc. Natl. Acad. Sci. U. S. A. 106 (2009) 8900–8905.
[42] R. Sen, H. Nagai, V.J. Hernandez, N. Shimamoto, Reduction in abortive transcription from the lambdaPR promoter by mutations in region 3 of the sigma70 subunit of *Escherichia coli* RNA polymerase, J. Biol. Chem. 273 (1998) 9872–9877.
[43] R. Sen, H. Nagai, N. Shimamoto, Polymerase arrest at the lambdaP(R) promoter during transcription initiation, J. Biol. Chem. 275 (2000) 10899–10904.
[44] Y. Berghofer-Hochheimer, C.Z. Lu, C.A. Gross, Altering the interaction between sigma70 and RNA polymerase generates complexes with distinct transcription-elongation properties, Proc. Natl. Acad. Sci. U. S. A. 102 (2005) 1157–1162.
[45] X. Han, C.L. Turnbough, Transcription start site sequence and spacing between the −10 region and the start site affect reiterative transcription-mediated regulation of gene expression in *Escherichia coli*, J. Bacteriol. 196 (2014) 2912–2920.
[46] S. Borukhov, V. Sagitov, C.A. Josaitis, R.L. Gourse, A. Goldfarb, Two modes of transcription initiation in vitro at the rrnB P1 promoter of *Escherichia coli*, J. Biol. Chem. 268 (1993) 23477–23482.
[47] R.S. Basu, B.A. Warner, V. Molodtsov, D. Pupov, D. Esyunina, C. Fernandez-Tornero, et al., Structural basis of transcription initiation by bacterial RNA polymerase holoenzyme, J. Biol. Chem. 289 (2014) 24549–24559.
[48] M.A. Lonetto, V. Rhodius, K. Lamberg, P. Kiley, S. Busby, C. Gross, Identification of a contact site for different transcription activators in region 4 of the *Escherichia coli* RNA polymerase sigma70 subunit, J. Mol. Biol. 284 (1998) 1353–1365.
[49] D. Dulin, D.L.V. Bauer, A.M. Malinen, J.J.W. Bakermans, M. Kaller, Z. Morichaud, et al., Pausing controls branching between productive and non-productive pathways during initial transcription in bacteria, Nat. Commun. 9 (2018) 1478.
[50] E.J. Strobel, J.W. Roberts, Regulation of promoter-proximal transcription elongation: enhanced DNA scrunching drives lambdaQ antiterminator-dependent escape from a sigma70-dependent pause, Nucleic Acids Res. 42 (2014) 5097–5108.
[51] A. Kulbachinskiy, A. Mustaev, Region 3.2 of the sigma subunit contributes to the binding of the 3′-initiating nucleotide in the RNA polymerase active center and facilitates promoter clearance during initiation, J. Biol. Chem. 281 (2006) 18273–18276.
[52] M. Imashimizu, N. Shimamoto, T. Oshima, M. Kashlev, Transcription elongation: heterogeneous tracking of RNA polymerase and its biological implications, Transcription. 5 (2014) e28285–1-10.
[53] S.A. Perdue, J.W. Roberts, Σ(70)-dependent transcription pausing in *Escherichia coli*, J. Mol. Biol. 412 (2011) 782–792.
[54] D. Dutta, K. Shatalin, V. Epshtein, M.E. Gottesman, E. Nudler, Linking RNA polymerase backtracking to genome instability in *E. coli*, Cell. 146 (2011) 533–543.
[55] T.S. Sankar, B.D. Wastuwidyaningtyas, Y. Dong, S.A. Lewis, J.D. Wang, The nature of mutations induced by replication–transcription collisions, Nature. 535 (2016) 178–181.
[56] D. Pupov, I. Kuzin, I. Bass, A. Kulbachinskiy, Distinct functions of the RNA polymerase sigma subunit region 3.2 in RNA priming and promoter escape, Nucleic Acids Res. 42 (2014) 4494–4504.
[57] M. Kashlev, E. Nudler, K. Severinov, S. Borukhov, N. Komissarova, A. Goldfarb, Histidine-tagged RNA polymerase of *Escherichia coli* and transcription in solid phase, Methods Enzymol. 274 (1996) 326–334.
[58] R.R. Burgess, Use of polyethyleneimine in purification of DNA-binding proteins, Methods Enzymol. 208 (1991) 3–10.
[59] H. Zhi, D.J. Jin, Purification of highly-active and soluble *Escherichia coli* sigma 70 polypeptide overproduced at low temperature, Methods Enzymol. 370 (2003) 174–180.

[60] M. Imashimizu, T. Oshima, L. Lubkowska, M. Kashlev, Direct assessment of transcription fidelity by high-resolution RNA sequencing, Nucleic Acids Res. 41 (2013) 9090–9104.
[61] M.L. Kireeva, L. Lubkowska, N. Komissarova, M. Kashlev, Assays and affinity purification of biotinylated and nonbiotinylated forms of double-tagged core RNA polymerase II from *Saccharomyces cerevisiae*, Methods Enzymol. 370 (2003) 138–155.
[62] M.L. Kireeva, Y.A. Nedialkov, G.H. Cremona, Y.A. Purtov, L. Lubkowska, F. Malagon, et al., Transient reversal of RNA polymerase II active site closing controls fidelity of transcription elongation, Mol. Cell 30 (2008) 557–566.